Journal of Solid State Chemistry **168,** 91–99 (2002)
doi:10.1006/jssc.2002.9692

Powder Neutron Diffraction and TEM Investigations of $Bi_{0.775}Ln_{0.225}O_{1.5}$ Oxide Conductors (*Ln*=La, Pr, Nd, Sm, Tb, Dy) with Rhombohedral Bi–Sr–O type: Structural Relationships with Monoclinic ε-$Bi_{4.86}La_{1.14}O_9$ Form

S. Obbade,*,[1] M. Huve,* E. Suard,† M. Drache,* and P. Conflant*

*Laboratoire de Cristallochimie et Physicochimie du Solide, UPRES A 8012, USTL-ENSCL, BP 108, 59652 Villeneuve d'Ascq Cedex, France; and †Institut Laue Langevin, Avenue des Martyrs, BP 38042 Grenoble Cedex 9, France

Received November 29, 2001; in revised form June 10, 2002; accepted July 15, 2002

Structural investigations of $Bi_{0.775}Ln_{0.225}O_{1.5}$ phases with rhombohedral Bi–Sr–O type, have been carried out using complementary techniques. Average crystal structures were refined from neutron diffraction powder data using the Rietveld method for *Ln* = La, Pr, Nd and Tb. The comparison with the monoclinic $Bi_{4.86}La_{1.14}O_9$ structure previously determined using the same technique has been done. For both types of structure, a piling of slabs constituted of a ($Bi_{(1)}$, *Ln*) oxide layer, inserted between two $Bi_{(2)}$ oxide layers, is observed. In the rhombohedral phases there are moreover oxide ions in the inter-slab spaces responsible for the well-known conductivity of these phases, while in the monoclinic $Bi_{4.86}La_{1.14}O_9$ structure, the absence of oxygen in the inter-slab spaces, is compensated with the presence of the $Bi_{(2)}$ lone pair electrons localized at a significant distance ($\cong$1.20 Å), which participate in the cohesion of the crystal structure. TEM study of $Bi_{0.775}Ln_{0.225}O_{1.5}$ samples, has confirmed the existence of superstructures for these phases and has allowed to propose two types (respectively for La and for Nd, Sm, Tb or Dy) of q_1* and q_2* modulation wave vectors.

Key Words: **bismuth lanthanide mixed oxides; rhombohedral Bi–Sr–O-type materials; powder neutron diffraction; transmission electron microscopy; electronic lone pair.**

INTRODUCTION

Numerous solid solutions, which adopt the Bi–Sr–O rhombohedral structural type (1), are obtained by cationic substitutions of M^{n+} for Bi^{3+} [*M* = alkaline earth (1–3), lanthanide or Y (4–7), alkaline earth + lead (8–9), La + Ce + M_{II} (M_{II} = Ba or Pb), La + M_{VI} + M_{II} (M_{VI} = Mo or W) (10)], in various Bi_2O_3-based oxide systems. Realized using X-ray diffraction data, the first structure determination, carried out on single crystal of the room temperature variety (β_2) of $Bi_{0.851}Sr_{0.149}O_{1.425}$ (11), was followed by different structural studies performed either on single crystal (3, 12, 13) or powder samples (14). Other techniques were also used for structural investigation of these phases' family: neutron diffraction on single crystal (15, 16) or on powdered material (17); electron microscopy in the Bi_2O_3–BaO (18) and Bi_2O_3–SrO or Bi_2O_3–CaO (12, 19) systems. Not only the existence of superstructure has been evidenced but moreover the electron diffraction (ED) study has detected systematic twinning of each crystal and the image's contrast has been identified with the existence of microdomains of ordering within a matrix of a normally disordered phase. The ED study of the Bi_2O_3–SrO and Bi_2O_3–CaO systems has revealed two kinds of superstructure depending on the Bi/Sr and Bi/Ca ratio.

All these materials crystallize in a rhombohedral symmetry and their average crystal structure was described with a hexagonal cell in $R\bar{3}m$ space group. The three-dimensional structure is constituted by a piling of slabs along the (001) axis. Each slab is constituted from two bismuth cationic layers $Bi_{(2)}$ surrounding a mixed layer containing the rest of bismuth $Bi_{(1)}$ and the other element(s) implicated in the phase. Two oxygen sites ($O_{(1)}$ and $O_{(2)}$) are located inside the slabs; the cohesion of layers in these blocks is principally due to $O_{(1)}$ ions which totally occupy a site located near the mixed cationic layers, while $O_{(2)}$ site near the $Bi_{(2)}$ layers is partially occupied. The remaining oxygen atoms as indicated by the compound formulae participate in the inter-block bonds. Each material exhibits a specific distribution of these anions over various sites depending on the nature and the ratio of the element(s) implicated in the phase. Most samples of

[1] To whom correspondence should be addressed. Fax: 33-320436814. E-mail: obbade@ensc-lille.fr.

0022-4596/02 $35.00

this family exhibit a β_1 high-temperature form with a hexagonal closely related structure. The $\beta_2 \rightarrow \beta_1$ transition occurs in all cases with a fast increase of conductivity; it has been clearly demonstrated for alkaline-earth-based phases that it corresponds to the migration of $O_{(2)}$-type ions (12, 16), toward the inter-slab space.

In the recent investigation of $Bi_{0.775}Ln_{0.225}O_{1.5}$ (Ln = La, Pr, Nd, Sm, Eu, Gd, Tb, Dy) oxide conductors (14), the Ln^{3+}_{VI} radius dependence of cell parameters and crystal structural characteristics (slab thickness, inter-slab distance, $O_{(2)}$ and $O_{(3)}$ occupancy factors) determined from powder X-ray diffraction data, and confirmed by the dependence of thermal expansion coefficients and electrical properties, suggested two different samples of subfamilies (La–Sm) and (Gd–Dy) with the intermediate Eu sample. This distinction was attributed to the existence of two kinds of ordering in the mixed cationic layers of the slabs.

The existence of these two cationic ordering types was confirmed from the evolution of the cell parameters according to the composition during the $Bi_{1-y}La_yO_{1.5}$ solid solution study (10). An investigation carrried out for one of the particular compositions, $Bi_{0.81}La_{0.19}O_{1.5}$, led to the identification of a new monoclinic form ε in system (20). A subsequent study has evidenced a solid solution domain with ε-type, for $0.15 \leq La/(La + Bi) \leq 0.325$ (21). The formation of this phase from the irreversible transformation of quenched β_1 on heating and the following transitions $\varepsilon \rightarrow \beta_2 \rightarrow \beta_1$ have been characterized by thermodiffractometry, conductivity measurements versus temperature, dilatometry and thermal analyses. The $\varepsilon \rightarrow \beta_2$ transition, irreversible for $0.15 \leq x \leq 0.275$, appears partly reversible for $0.3 \leq x \leq 0.325$. *Ab initio* crystal structure determination of ε-$Bi_{0.81}La_{0.19}O_{1.5}$ phase has been realized from powder neutron diffraction data, in monoclinic cell ($a = 9.4956(3)$Å, $b = 3.9742(1)$ Å, $c = 7.0425(2)$ Å, $\beta = 104.700(2)^\circ$ and $Z = 6$) with $P2/c$ space group. In this case, the crystal structure is formed by a piling of slabs according to the monoclinic a-axis. Each cell corresponds to one slab containing a mixed $Bi_{(1)0.86}La_{1.14}$ cationic layer ($M_{(1)}$) sandwiched between two bismuth layers ($Bi_{(2)}$). The cohesion of the cations in the slabs results from the presence of the oxygen atoms distributed over three sites. Six $O_{(1)}$ and two $O_{(2)}$ atoms form a slightly distorted cubical polyhedron around the mixed cationic site. $Bi_{(2)}$ atoms are surrounded by seven oxygen atoms (one $O_{(1)}$ and three $O_{(2)}$, with a third kind ($O_{(3)}$) in a very distorted polyhedron. The important delocalization of $Bi_{(2)}$ lone pairs toward the inter-slabs spaces leads to significant bonds with the adjacent slabs and to the cohesion of the structure

This paper deals with the crystal structural investigation of Bi–*Ln*–O mixed oxides using two complementary techniques: powder neutron diffraction and transmission electron microscopy (TEM). The neutron diffraction study allows to localize a supplementary oxygen site, partially occupied, which the X-ray diffraction was unable to discover. The determination of the oxygen occupancy factors, with a good precision, allows better understanding of the specific anionic conductivity mechanism in these materials. A discussion on the crystal structure relationships with the monoclinic ε-phase, recently isolated, is given. The second technique has confirmed the existence of superstructures for these phases and has allowed to propose two types of modulation.

EXPERIMENTAL

$Bi_{0.775}Ln_{0.225}O_{1.5}$ powder samples (Ln = La, Pr, Nd, Sm, Tb and Dy) have been synthesized by solid-state reaction of Bi_2O_3 and Ln_2O_3 (99.9%) obtained from the commercial products preheated at various temperatures for 15 h (Bi_2O_3: 600°C; rare-earth oxides: 875°C for Ln = La, Pr, Nd, Sm and 620°C for Ln = Tb and Dy). Stoichiometric proportions of reactants were accurately weighed and intimately ground in an agate mortar. Each mixture was transferred into a gold crucible and heated at 815°C for two 15 h treatments. The samples were then annealed at 610°C for 60 h. The end of the synthesis process, characterized for each sample by the obtaining of the pure β_2 hexagonal variety, was checked by X-ray diffraction using a Guinier de Wolff camera (Cu$K\alpha$ radiation).

In the previous crystal structural study of $Bi_{0.775}Ln_{0.225}O_{1.5}$ compounds (14), using X-ray diffraction data, the presence of heavy atoms as Bi and *Ln* in these materials did not allow the localization of all oxygen sites, which are necessary to understand the oxide conduction mechanism in these materials. Then, a similar study by neutrons diffraction was realized for lanthanide atoms possessing a weak absorption cross section (Ln = La, Pr, Nd and Tb). The neutron powder diffraction patterns were collected at room temperature using the high-resolution D1A powder diffractometer in the (*Institute Laue Langevin* (ILL)), Grenoble. The incident neutron wavelength 1.911 Å, was selected from the (113) plane of germanium single-crystal monochromator. About 10 g of each sample was enclosed in a vanadium cylindrical 8-mm-diameter can. The counter was moved by steps of 0.05 in the range $10^\circ \leq 2\theta \leq 160^\circ$. The counting times were 15 h for each compound and a total of 3000 data points were recorded. Both neutron diffraction patterns were refined by Rietveld method (22, 23), using the FullProf program (24), a strongly modified version of the Young and Wiles refinement program (25, 26). A Gaussian function was chosen to generate the line shape of the diffraction peaks. The Gaussian component has widths given by the function $(FWHM)^2 = U\tan^2\theta + V\tan\theta + W$ (27), where U, V, and W are refineable parameters. The coherent scattering lengths used were 8.240, 4.580, 7.690, 7.38, 8.526 and 5.805 fm for La,

Pr, Nd, Tb, Bi and O respectively. The background was defined by fifth-order polynomial in 2θ and was refined simultaneously with the other profile parameters. Cell dimensions and crystal structural parameters were refined, with independent refinement of the profile parameters, i.e., peak shapes, background parameters, zero point correction and scale factors. At the end of the refinement, the good fitting between observed and calculated data was indicated by the significant values of the profile reliability factors (R_p, R_{wp}) and the average crystal structure model quality factors (R_F, R_{bragg}).

From atomic positions obtained by neutron diffraction refinement, the location of the bismuth lone pair ($\mathbf{d} = \alpha E$) was carried out with the program HYBRIDE (28) based on the algorithm of Verbaere *et al.* (29), in which the local electric field (E) in the crystal is calculated by the Ewald method (30), where the ion bismuth polarizability coefficient $\alpha(Bi^{3+})$ was obtained from the Clausius–Masotti formula and refraction indexes of several compounds containing the Bi^{3+} ion.

Electron diffraction patterns and high-resolution images of all $Bi_{0.775}Ln_{0.225}O_{1.5}$ synthesized samples (Ln = La, Nd, Sm, Tb and Dy) were obtained on a Jeol 200CX and a Jeol 4000EX with a point resolution of 1.7 Å. In each case, the material was crushed and dispersed on a holey carbon film deposited on a Cu grid.

RESULTS AND DISCUSSION

Crystal structure

Having refined the profile and unit cell parameters using the *pattern matching* option of the Fullprof program, the refinement of average crystal structure was carried out in the centrosymmetric $R\bar{3}m$ space group, taking as starting model the powder X-ray crystal structure investigation of $Bi_{0.775}Ln_{0.225}O_{1.5}$ (two cationic sites and three sites of oxygen) (14). $Bi_{0.775}Pr_{0.225}O_{1.5}$ compound has been chosen for the first refinement, because Bi and Pr are the elements possessing the biggest difference between the coherent scattering lengths, so best resolution. The occupation factors of Bi and Pr atoms in the mixed site were refined with a linear constraint to comply with the chemical formula. After several refinement cycles, it appeared clearly that the occupancy factors in the mixed site correspond exactly to the nominal chemical formula, so for the other compounds these occupation factors were fixed in agreement with the formula. The refinement of this crystal structure model followed by a Fourier difference analysis revealed a new site of oxygen in agreement with the X-ray investigation (14).

The refined crystal structures were characterized by a full occupancy of Bi 6c site (0, 0, z) and a statistical distribution of Bi and Ln atoms in the site 3a (0,0,0), with occupancy coefficients fitting the composition $Bi_{0.775}Ln_{0.225}O_{1.5}$. The oxide ions are distributed in two sorts of sites, 6c (0, 0, z) for $O_{(1)}$, $O_{(2)}$ and $O_{(3)}$ atoms, while the oxygen $O_{(4)}$ is in site 18 h (x, $2x$, z), only the $O_{(1)}$ site is fully occupied. The occupancy factors of the oxygen sites $O_{(2)}$, $O_{(3)}$ and $O_{(4)}$ were refined under a linear constraint to comply with the chemical formula. In the final refinement, anisotropic thermal parameters were refined for all atoms. Crystal data and details of refinements are collected in Table 1. Final atomic positions, occupancy factors and equivalent thermal coefficients are reported in Table 2. The anisotropic thermal factors and selected inter-atomic distances

TABLE 1
Crystal and Refinement Parameters from Neutron Diffraction Patterns

Chemical formula	$Bi_{0.775}La_{0.225}O_{1.5}$	$Bi_{0.775}Pr_{0.225}O_{1.5}$	$Bi_{0.775}Nd_{0.225}O_{1.5}$	$Bi_{0.775}Tb_{0.225}O_{1.5}$
Formula weight, g/mol	217.2	217.7	218.4	221.7
Crystal system	Rhombohedral	Rhombohedral	Rhombohedral	Rhombohedral
Space group	*R*-3*m*	*R*-3*m*	*R*-3*m*	*R*-3*m*
Unit cell	Hexagonal	Hexagonal	Hexagonal	Hexagonal
a (Å)	4.0253(1)	3.9989(1)	3.9926(1)	3.9648(1)
c (Å)	27.6004(9)	27.5265(7)	27.4687(7)	27.3298(8)
v (Å)^3	387.29(1)	381.20(2)	379.21(2)	372.05(2)
Unit formula (Z)	9	9	9	9
Sample description	Yellow powder	Yellow powder	Yellow powder	Yellow powder
Half-width parameters				
U	0.327(9)	0.200(7)	0.165(6)	0.232(9)
V	−0.568(9)	−0.427(6)	−0.347(9)	−0.449(9)
W	0.412(9)	0.345(9)	0.300(7)	0.347(9)
R factors				
R_{exp}	0.026	0.024	0.027	0.030
R_p	0.062	0.045	0.053	0.052
R_{wp}	0.085	0.060	0.073	0.069
R_F	0.063	0.071	0.071	0.079
R_B	0.082	0.093	0.082	0.091

TABLE 2
Final Refined Atomic Positions, Occupancy Factors and Equivalent Thermal Displacements B_{eq} (Å^2)

Atom	Site	x	y	z	B_{eq} (Å^2)[a]	Occup.
$Bi_{0.775}Nd_{0.225}O_{1.5}$						
Bi_1/La	3a	0	0	0	1.65	0.975/2.025
Bi_2	6c	0	0	0.22475(7)	2.01	6
O_1	6c	0	0	0.2997(1)	2.82	6
O_2	6c	0	0	0.0934(2)	5.73	4.45(5)
O_3	6c	0	0	0.4400(9)	3.53	1.78(5)
O_4	18h	0.201(7)	0.402(7)	0.496(1)	5.38	1.27(5)
$Bi_{0.775}Pr_{0.225}O_{1.5}$						
Bi_1/Pr	3a	0	0	0	1.80	0.97/2.03(2)
Bi_2	6c	0	0	0.22433(7)	1.59	6
O_1	6c	0	0	0.3005(1)	2.27	6
O_2	6c	0	0	0.0911(2)	4.46	4.46(4)
O_3	6c	0	0	0.4455(4)	4.40	1.77(4)
O_4	18h	0.200(7)	0.400(7)	0.491(2)	5.37	1.27(4)
$Bi_{0.775}Nd_{0.225}O_{1.5}$						
Bi_1/Nd	3a	0	0	0	1.26	0.975/2.025
Bi_2	6c	0	0	0.22478(8)	2.03	6
O_1	6c	0	0	0.3009(1)	2.57	6
O_2	6c	0	0	0.0910(2)	4.26	4.48(5)
O_3	6c	0	0	0.4427(6)	4.60	1.76(5)
O_4	18h	0.210(8)	0.420(8)	0.490(1)	5.30	1.26(5)
$Bi_{0.775}Tb_{0.225}O_{1.5}$						
Bi_1/Tb	3a	0	0	0	1.73	0.974/2.025
Bi_2	6c	0	0	0.22456(8)	1.27	6
O_1	6c	0	0	0.3025(2)	2.39	6
O_2	6c	0	0	0.0878(2)	3.87	4.24(5)
O_3	6c	0	0	0.4481(5)	4.39	1.88(5)
O_4	18h	0.200(8)	0.400(8)	0.491(1)	5.02	1.38(5)

[a] $B_{eq}\frac{4}{3}\sum_i \sum_j \beta_{ij} a_i a_j$.

are, respectively, presented in Tables 3 and 4. At the end of refinement, the good agreement between the refined model and the real crystal structure was indicated by the comparison between the calculated and observed patterns; an example is given for Pr compound in Fig. 1.

As a result of the limited number of samples examined using neutron diffraction data, it is not possible to distinguish from the structural results, the two series of rhombohedral-type $Bi_{0.775}Ln_{0.225}O_{1.5}$ materials evidenced in the previous study (14). A slight increase of the distances to the mixed layers, for $Bi_{(2)}$, $O_{(1)}$, $O_{(2)}$ and $O_{(4)}$ atoms, with the increase of the *Ln* size from Tb to La, is observed. In accordance with the description of the rhombohedral structure (3, 12–14) each slab is delimited with two $Bi_{(2)}$ layers. For the lanthanum compound, $O_{(3)}$ atoms appear located inside the slabs, contrarly to what is observed with other samples.

The rare-earth atoms nature does not influence the occupation in the oxygen sites partially occupied ($O_{(2)}$, $O_{(3)}$ and $O_{(4)}$), which remains constant when we change the lanthanide in the mixed layer. $O_{(1)}$ and $O_{(2)}$, sites common to $Bi_{(1)}$ and $Bi_{(2)}$ environment, which assure the cohesion between layers in blocks $Bi_{(2)}$–$Bi_{(1)}$–$Bi_{(2)}$, are strongly occupied ($O_{(1)}$–100% and $O_{(2)} \sim 75\%$), whereas $O_{(3)}$ and $O_{(4)}$ sites which are respectively on the periphery and outside of these cationic blocks, are weakly occupied ($O_{(3)} \sim 30\%$ and $O_{(4)} \sim 7\%$) and assure the cohesion between the slabs. These observations confirm that the specific oxide ion conductivity observed in these materials is mainly assured by oxygen atoms $O_{(3)}$ and $O_{(4)}$ which move between the blocks.

It is also interesting to compare the average crystal structure with that obtained for the monoclinic phase, which was recently determined *ab initio* from powder neutron diffraction data (21). The monoclinic compound contains only six $Bi_{0.81}La_{0.19}O_{1.5}$ units by cell, but the crystal structure has a close relationship with that of the rhombohedral phases and is formed by similar cationic layers and blocks. In Fig. 2, we present a projection of the two crystal structures perpendicular to the cationic layers.

TABLE 3
Anisotropic Thermal Displacement Coefficients ($\beta_* 10^4$) for $Bi_{0.775}Ln_{0.225}O_{1.5}$ (For all atoms $\beta_{11}=\beta_{22}=2\beta_{12}$ and $\beta_{13}=\beta_{23}=0$, except for O(4) ($\beta_{11}=\beta_{22}$ and $\beta_{13}=-\beta_{23}$)

Ln		La	Pr	Nd	Tb
$Bi_{(1)}$	β_{11}	243(34)	231(44)	144(34)	259(44)
	β_{33}	8.5(6)	10.5(8)	7.9(6)	9.1(8)
$Bi_{(2)}$	β_{11}	514(24)	421(21)	547(27)	404(27)
	β_{33}	3.4(3)	2.5(3)	2.9(3)	0.0(4)
$O_{(1)}$	β_{11}	704(39)	603(35)	627(38)	644(46)
	β_{33}	5.3(5)	3.4(4)	5.7(5)	3.7(6)
$O_{(2)}$	β_{11}	1454(85)	1126(72)	1156(95)	925(92)
	β_{33}	10(1)	8(1)	6(1)	10(1)
$O_{(3)}$	β_{11}	342(232)	1476(201)	1111(190)	931(171)
	β_{33}	24(3)	4(2)	11(3)	11(4)
$O_{(4)}$	β_{11}	1009(292)	1009(274)	1009(302)	1009(319)
	β_{33}	10(6)	10(5)	10(7)	10(6)
	β_{12}	4(3)	4(3)	3(2)	103(80)
	β_{13}	1(5)	2(3)	1(3)	1(3)

The distances to the mixed [$Bi_{(1)}$,La] layers (B' layers in $Bi_{0.81}La_{0.19}O_{1.5}$), of $Bi_{(2)}$ layers and of $O_{(2)}$ atoms, quite agree with the corresponding parameters in the rhombohedral phases. Similar to what was observed for the rhombohedral lanthanum phase, the oxygen atom $O_{(3)}$ is located near the $Bi_{(2)}$ layers inside the slabs of the monoclinic phase, but there are not any atom $O_{(4)}$ in the inter-slabs spaces. The conductivity decrease of about one decade, when successive rhombohedral and monoclinic phases are examined, indicates that $\beta_2 - \sigma$ results predominantly from $O_{(4)}$ ions mobility. The absence of this oxygen in the monoclinic phase is then compensated with a significant distance of the bismuth lone pair ($Bi_{(2)}$–Lp) to occupy this vacuum. For rhombohedral phases, the lone pairs reported in Table 5, are oriented perpendicular to the slabs along the *c*-axis direction; whatever the considered rare earth, the distance between a $Bi_{(2)}$ atom and the corresponding lone pair is similarly the same (0.585–0.620 Å). Cohesion of the structures results from interactions between electrons of lone pairs and oxide ions $O_{(4)}$ of the inter-slabs spaces, and $Bi_{(2)}$ cations of the neighbor slabs. For monoclinic $Bi_{0.81}La_{0.19}O_{1.5}$ sample, alternating orientations of the lone pairs for the $Bi_{(2)}$ cations are observed with a distances $d=1.22$ Å. Such an unusually important lone pair delocalization results from the absence of $O_{(4)}$ ions between blocks; thus, only the electrons of the lone pairs assure the inter-slabs cohesion.

TABLE 4
Selected Interatomic Distances for $Bi_{0.775}Ln_{0.225}O_{1.5}$

	Ln			
	La	Pr	Nd	Tb
($Bi_{(1)}$,*Ln*)–$O_{(1)}$	2.502(2)	2.479(1)	2.472(2)	2.440(2)
($Bi_{(1)}$,*Ln*)–$O_{(2)}$	2.577(5)	2.508(5)	2.499(6)	2.400(7)
$Bi_{(2)}$–$O_{(1)}$	2.070(5)	2.099(4)	2.090(5)	2.129(5)
$Bi_{(2)}$–$O_{(2)}$	2.362(1)	2.361(1)	2.355(1)	2.360(2)
$Bi_{(2)}$–$O_{(3)}$	2.325(1)	2.310(1)	2.305(1)	2.295(1)
$Bi_{(2)}$–$O_{(4)}$	2.66(4)	2.73(3)	2.62(3)	2.71(4)

Transmission Electron Microscopy Study (TEM)

The TEM study of the $Bi_{0.775}Ln_{0.225}O_{1.5}$ mixed oxides (*Ln* = La, Nd, Sm, Tb and Dy) has been undertaken in order to obtain some information about the evolution of the modulation versus the *Ln* nature, for a large lanthanide radius variation. Because of the micaceous behavior of these crystals, the crystal plates are [001] zone axis oriented, and zone axis containing the *c* parameter can not be obtained, because the tilting possibilities on the microscope are limited.

(a) Systematic Existence of Twin ?

The systematic existence of twin detected by Tilley in the Bi_2O_3–BaO (18) system is not observed in the system studied. The twinning phenomenon is dependent on the substituting element and the synthesis conditions. As no twin is observed for La, Tb, Dy compounds, an almost systematic twin is detected in the [−111] zone axis for Sm and Nd phases (Fig. 3). The electron diffraction pattern (EDP) of a rarely not twinned crystal of Sm-substituted compounds (Fig. 3a) is helpful to identify the twin (Fig. 3b). It consists of a rotation along the (−111) direction by about 30° (Fig. 3d). This twin phenomenon is identical for the Sm, Nd as well as for the Ba compounds [18].

(b) Modulation and Substituted Element

The [−111] ED patterns are identical for the Sm, Nd, Tb, Dy phases (Fig. 4) and can be characterized with one modulation wave vector:

$$q^* = \tfrac{1}{7}(3a^* - 2b^* + 5c^*).$$

This is in accordance with what has been already found for Sr and Ca system and called the S1 phases (19). The first-order Laue zone is not visible in the perfect [−111] zone axis orientation and so the access of the third parameter of the superstructure is not possible. Curiously, the La phases exhibit a different modulation in this [−111] zone axis (Fig. 4b) with modulation wave vectors:

$$q^* = \tfrac{1}{12}(3a^* - 2b^* + 5c^*).$$

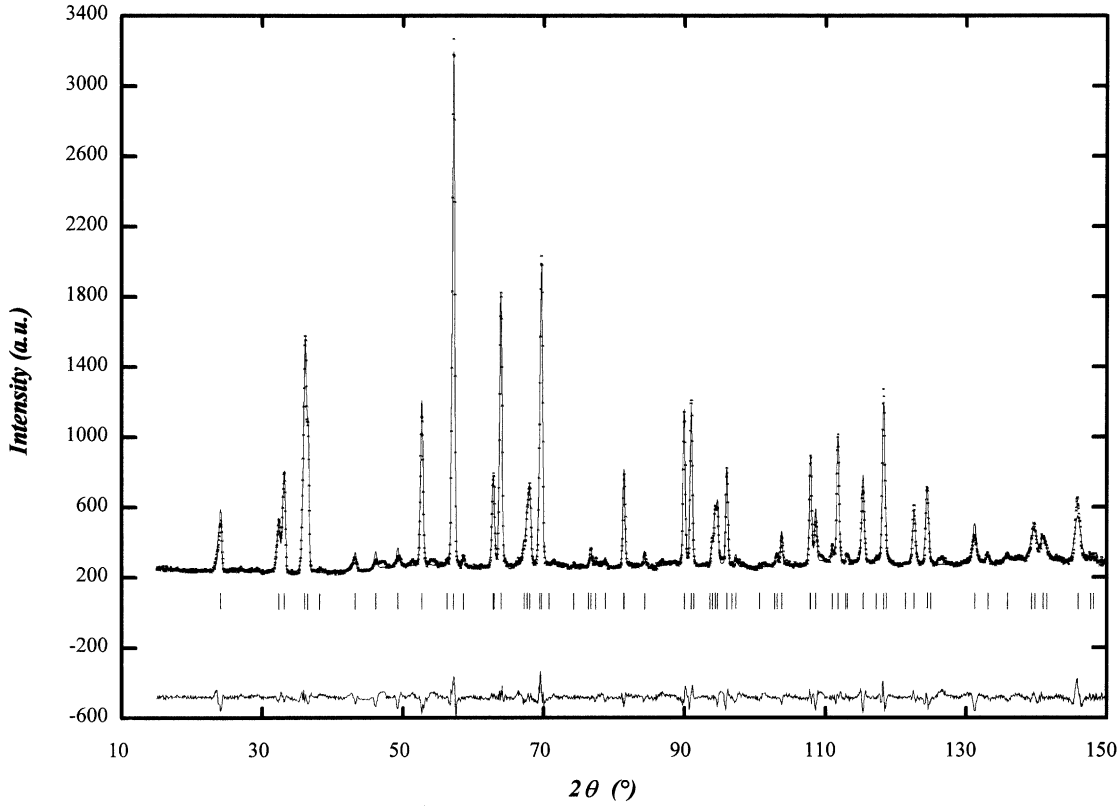

FIG. 1. Observed and calculated neutron diffraction pattern for $Bi_{0.775}Pr_{0.225}O_{1.5}$.

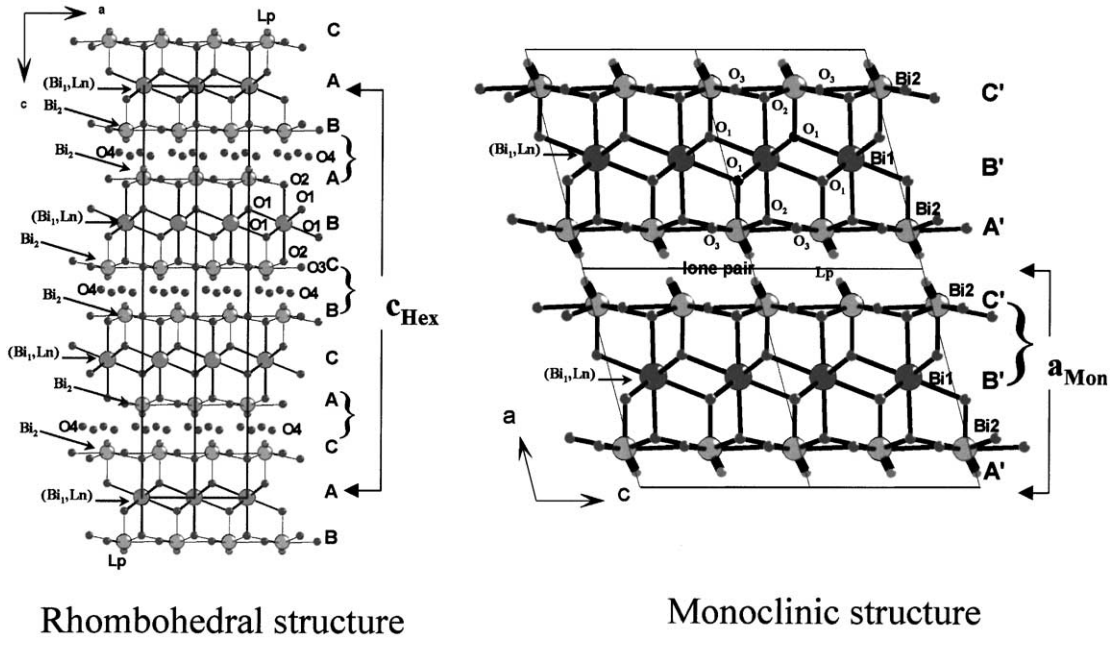

FIG. 2. Comparison of rhombohedral and monoclinic structures.

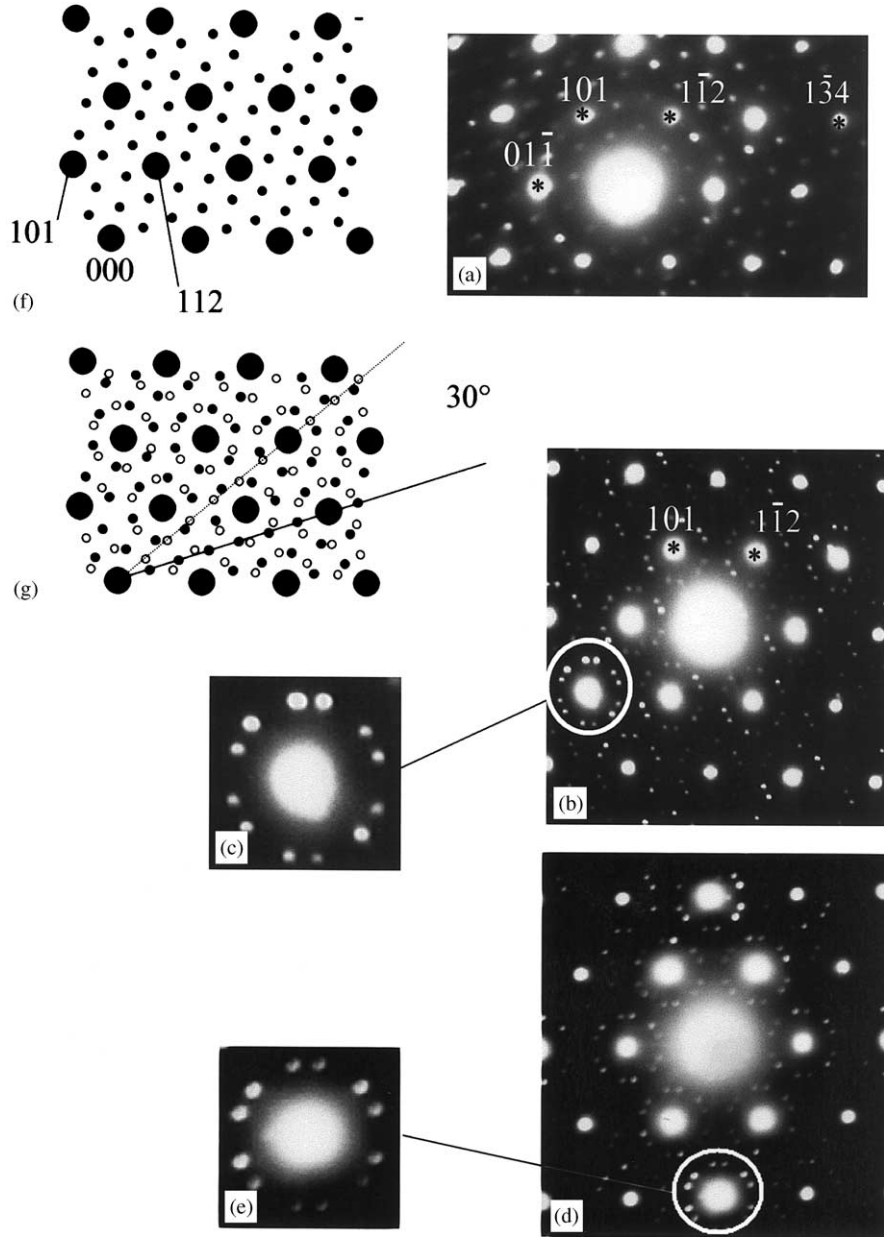

FIG. 3. Twinning phenomenon. Sm compound [−111] zone axis (a) of a very rarely not-twinned crystal (b) of a twinned crystal, (c) enlargement of a part of the EDP of (b). Nd phases [−111] zone axis–(d) of a twinned crystal, (e) enlargement of a part of the EDP of (d). Schematic representation of the twin in the [−111] zone axis (f) without twin, (g) with a twin resulting from a rotation of 30° around [−111].

Briefly, the modulation vector seems to be unaffected by the nature of the substituting element for investigated materials, except for the La element which seems to have a different behavior.

(c) Image of the La Phase

In Fig. 5, we can see for the La compound, a zone axis where the modulation is well established, that is the [15–1] zone axis (Fig. 5a). The modulation can be defined by one vector:

$$q^* = \tfrac{1}{12}(a^* + 2b^* + 11c^*).$$

At first glance, the image seems to be the result of a superposition of some different crystals (Fig. 5b). But a careful examination establishes a continuity between the three zones labeled 1, 2, 3, which is not compatible with a random superposition of three crystals. Consequently, there is only one crystal with a different thickness. The

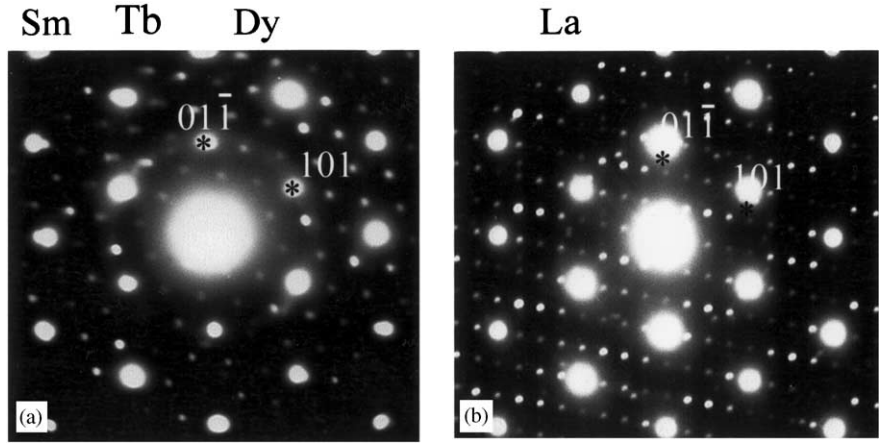

FIG. 4. [−111] EDP of (a) Sm, Tb, Dy and (b) La-doped compounds. The modulation is the same for all compounds except for the La-doped phases.

thinner area (labeled 1) does not reveal any sign of superstructure as the corresponding Fourier transform (FT) attests (Fig. 5c). In the thicker zone (labeled 2) the superstructure is well established in accordance with the corresponding FT (Fig. 5d) and the enlarged image (Fig. 5e) in which the superstructure is represented by the form. The origin of this superstructure is attributed to an ordering between the different cations in the mixed layer (18).

In conclusion, the La phase seems to have a different behavior compared to those with other elements like Nd, Sm, Tb, Dy, Sr or Ca, because it leads to a different superstructure phenomenon. This could indicate that Sm sample identified as the limit term of the first subfamily from the previous investigation [14] belongs in fact to the second subfamily. It will be very interesting to study these modulations by means of X-ray diffraction on single crystal in order to

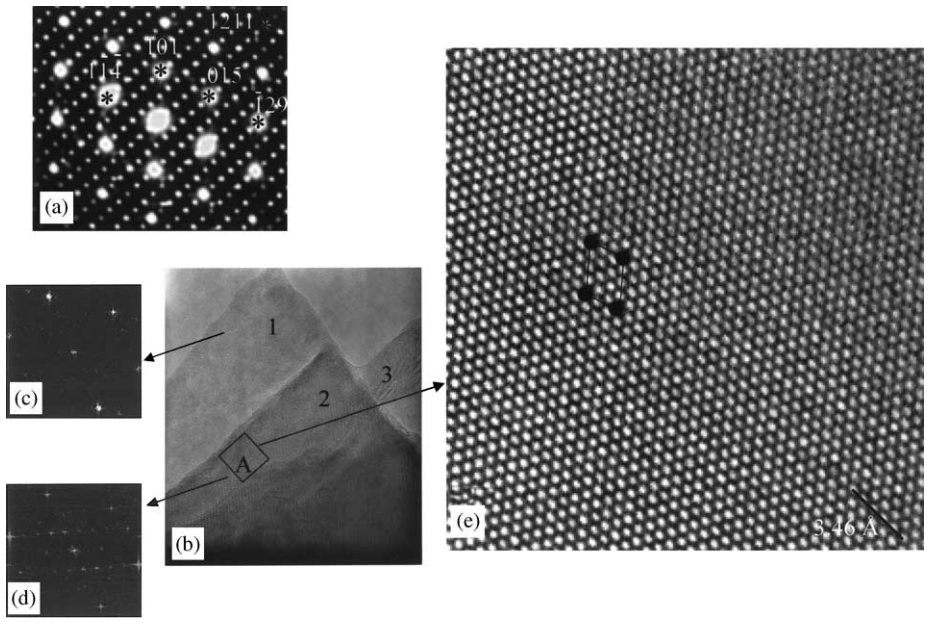

FIG. 5. (a) [15−1] zone axis pattern where the modulation is well established; (b) corresponding image where different thicknesses are observed. In the thinner part no superstructures are observed as the (c) Fourier Fonction Transfert (FFT) attests. In the thicker part (d) the corresponding FFT shows the superstructure phenomenon. (e) Enlargement of the domain A of (b). The superstructure is highlighted and schematically represented by the black lines.

TABLE 5
Lone Pair (Lp) Position*, Distances (Lp–O) <3Å and Angles (Lp–Bi–O)

	Lp position	Lp–O	distances (Å)	Lp–Bi–O Angles (deg)
$Bi_{0.775}La_{0.225}O_{1.5}$		Lp–Bi(2)	0.615(9)	
		Lp–O(1)	2.685(3)	180
	$x=0$	Lp–O(2)	2.544(6)	100.24(4)
	$y=0$	Lp–O(3)	2.418(7)	91.30(6)
	$z=0.202(4)$	Lp–O(4)	2.307(8)	49.76(5)
$Bi_{0.775}Pr_{0.225}O_{1.5}$		Lp–Bi(2)	0.587(9)	
		Lp–O(1)	2.686(2)	180
	$x=0$	Lp–O(2)	2.549(5)	102.03(5)
	$y=0$	Lp–O(3)	2.362(6)	87.84(5)
	$z=0.203(4)$	Lp–O(4)	2.375(7)	47.46(6)
$Bi_{0.775}Nd_{0.225}O_{1.5}$		Lp–Bi(2)	0.620(9)	
		Lp–O(1)	2.710(2)	180
	$x=0$	Lp–O(2)	2.556(5)	101.84(5)
	$y=0$	Lp–O(3)	2.381(4)	89.44(4)
	$z=0.202(4)$	Lp–O(4)	2.272(6)	50.51(6)
$Bi_{0.775}Tb_{0.225}O_{1.5}$		Lp–Bi(2)	0.611(9)	
		Lp–O(1)	2.74(3)	180
	$x=0$	Lp–O(2)	2.58(4)	104.05(7)
	$y=0$	Lp–O(3)	2.33(5)	85.91(5)
	$z=0.202(4)$	Lp–O(4)	2.34(6)	47.32(6)

have precise information about the origin of these phenomena.

ACKNOWLEDGMENTS

The authors are very grateful to Mrs. Nora Djelal for her help with samples syntheses.

REFERENCES

1. P. Conflant, J. C. Boivin, and D. Thomas, *J. Solid State Chem.* **18,** 133 (1976).
2. R. Guillermo, P. Conflant, J. C. Boivin, and D. Thomas, *Rev. Chim. Minér.* **15,** 153 (1978).
3. P. Conflant, J. C. Boivin, G. Nowogrocki, and D. Thomas, *Solid State Ionics* **9/10,** 295 (1983).
4. A. Watanabe and T. Kikuchi, *Solid State Ionics* **21,** 287 (1986).
5. A. Watanabe, *Solid State Ionics* **34,** 35 (1989).
6. P. Conflant, C. Follet-Houttemane, and M. Drache, *J. Mater. Chem.* **1,** 649 (1991).
7. A. Watanabe, M. Drache, J. P. Wignacourt, P. Conflant, and J. C. Boivin, *Solid State Ionics* **67,** 25 (1993).
8. A. El Harrak, P. Conflant, M. Drache, and J. C. Boivin, *J. Chim. Phys.* **88,** 2281 (1991).
9. M. Drache, P. Conflant, and J. C. Boivin, *Solid State Ionics* **57,** 245 (1992).
10. M. Drache, J. P. Wignacourt, and P. Conflant, *J. Solid State Chem.* **149,** 341 (2000).
11. P. Conflant, J. C. Boivin, and D. Thomas, *J. Solid State Chem.* **35,** 192 (1980).
12. P. Conflant, Thesis, University of Lille, 1985.
13. M. Drache, J. P. Wignacourt, and P. Conflant, *Solid State Ionics* **86–88,** 289 (1996).
14. M. Drache, S. Obbade, J. P. Wignacourt, and P. Conflant, *J. Solid State Chem.* **142,** 349 (1999).
15. D. Mercurio, M. El Farissi, J. C. Champarneaud-Mesjard, B. Frit, and P. Conflant, *J. Solid State Chem.* **80,** 133 (1989).
16. D. Mercurio, J. C. Champarneaud-Mesjard, B. Frit, P. Conflant, J. C. Boivin, and T. Vogt, *J. Solid State Chem.* **112,** 1 (1994).
17. S. K. Blower and C. Greaves, *Mater. Res. Bull.* **23,** 765 (1988).
18. R. J. D. Tilley, *J. Solid State Chem.* **41,** 233 (1982).
19. R. L. Withers and H. Rossell, *J. Solid State Chem.* **118,** 66 (1995).
20. M. Drache, J. P. Wignacourt, and P. Conflant, *J. Solid State Chem.* **151,** 281 (2000).
21. S. Obbade, M. Drache, and P. Conflant, *J. Solid State Chem.* **162,** 341 (2001).
22. H. M. Rietveld, Acta Crystallogr. **22,** 151 (1967).
23. H. M. Rietveld, J. Appl. Crystallogr. **2,** 65 (1969).
24. J. Rodriguez-Carvajal, M. T. Fernandez-Diaz, and J. L. Martinez, *J. Phys:. Condens. Mater.* **3,** 3215 (1991).
25. D. B. Wiles and R. A. Young, *J. Appl. Crystallogr.* **14,** 149 (1981).
26. D. B. Wiles and R. A. Young, *J. Appl. Crystallogr.* **15,** 430 (1982).
27. C. Caglioti, A. Paoletti, and E. P. Ricci, *Nucl. Instrum. Methods* **3,** 223 (1958)
28. E. Morin, G. Wallez, S. Jaulmes, J. C. Couturier, and M. Quarton, *J. Solid State Chem.* **137,** 283 (1998).
29. A. Verbaere, R. Marchand, and M. J. Tournoux, *J. Solid State Chem.* **23,** 383 (1978).
30. P. P. Ewald, *Ann. Phys.* **64,** 253 (1921).